A Sensitivity Analysis of Wave Energy Converter Model Predictive Control Systems With Wave Excitation Force Estimation and Prediction

Zechuan Lin, *Student Member, IEEE*, Xuanrui Huang, *Member, IEEE*, Xi Xiao, *Member, IEEE*, and John V. Ringwood, *Fellow, IEEE*

***Abstract*— Understanding the sensitivity of energy-maximizing control for wave energy converters (WECs), to various model errors, is crucial for application. Many advanced WEC controllers, especially model predictive control (MPC)-like controllers, require estimation and prediction of wave excitation force (WEF). However, previous studies only focus on the controller in isolation, without considering the error coupling effects when a complete estimation–prediction loop is involved. In this study, it is revealed through numerical analysis that the complete MPC system has sensitivity behavior completely different from the isolated MPC; under certain model errors, the system can become particularly unpredictable, exhibiting potential instability and self-locking phenomena, which cannot be observed from the examination of control sensitivity alone. Meanwhile, different tuning options for the WEF estimator and predictor are examined, where the accuracy–robustness tradeoff is shown to be critical for performance amelioration under errors. Based on the analysis, this study challenges the widely assumed "separation principle" of WEF estimation/prediction and WEC control, highlights the importance of incorporating a complete estimation–prediction loop in sensitivity examination, and draws practical guidelines for WEC control application.**

***Index Terms*— Model predictive control (MPC), sensitivity analysis, wave energy.**

I. Introduction

ENERGY-MAXIMIZING control technologies are recognized as one of the most effective approaches to boost the energy capture of wave energy converters (WECs), offering a promising solution for a further reduction of the levelized cost of wave energy (LCoE) [1]. Conventional WEC controllers are typically designed to approach the impedance-matching condition from a linear perspective, such as the approximate complex-conjugate (ACC) (or "reactive") control and approximate optimal velocity tracking (AVT) control [2]. In the last decade, controllers based on numerical optimization, represented by model predictive control (MPC), have seen rapid development, primarily due to their capability of uniformly handling multiple system models, objectives, and constraints [3]. In general, the majority of these controllers fall into the category of model-based control, for which the issue of control robustness against model errors is critical, and that is particularly the case for WEC controllers, due to the following factors:

1) Linear hydrodynamic models [4], widely used for WEC control, lose their accuracy under exaggerated WEC motion driven by energy-maximizing control [5] and cannot consider other nonlinear effects, such as mechanical friction [6].
2) The model complexity that WEC controllers can manage is restricted: linear ACC and AVT [2] require a linear model and, for optimization-based controllers, a linear model remains preferable since it leads to an acceptable online computational burden [3].
3) To achieve such *control-oriented modeling* [7], a system identification process is typically required, and the obtained linear model parameters are also subjected to identification errors.
4) Energy-maximizing control of WECs exhibits sensitivity behavior significantly different from conventional stabilizing or tracking controllers [8]. In the latter case, closed-loop control robustness can be enhanced through feedback, while that is not generally true for WEC control, due to the energy maximizing objective.

In [8], the sensitivity properties of linear ACC and AVT are examined both analytically and numerically. However, the target controllers are confined to the linear category, while the MPC-like controllers, especially those taking the maximization of energy as the objective function, have not been studied.

The implementation of WEC MPC requires the acquisition of present and future wave information. A preferred approach is to estimate the instantaneous wave excitation force (WEF) as an unknown input, purely based on a model of the system and available measurements [9], and predict future WEF using time-series models [10]; in such a way, no additional deployment/maintenance of wave observing system is required, and the difficulty of wave direction identification [11] is avoided. Currently, the majority of WEC controllers are designed based on a perfect knowledge of WEF, which implies the assumption

Manuscript received 12 February 2024; revised 13 February 2024, 15 May 2024, 16 May 2024, and 16 August 2024; accepted 22 August 2024. Date of publication 30 September 2024; date of current version 31 December 2024. This work was supported in part by the National Natural Science Foundation of China under Grant 52337002 and in part by the National Key Research and Development Program of China under Grant 2020YFE0205400. Recommended by Associate Editor E. Capello. *(Corresponding author: Xi Xiao.)*

Zechuan Lin, Xuanrui Huang, and Xi Xiao are with the Department of Electrical Engineering, Tsinghua University, Beijing 100084, China (e-mail: zechuanlin@126.com; hxr503@gmail.com; xiao_xi@tsinghua.edu.cn).

John V. Ringwood is with the Centre for Ocean Energy Research (COER), Maynooth University, County Kildare, Maynooth, W23 A3HY Ireland (e-mail: john.ringwood@mu.ie).

Digital Object Identifier 10.1109/TCST.2024.3456689

of a "separation principle" of estimation/prediction and control [12]. However, as can be seen in Fig. 1, that assumption becomes problematic under model errors, which now affect not only the MPC solution *but also* WEF estimation, with the estimation error *propagating* to WEF prediction and finally to the MPC input; in other words, the roles of estimation, prediction, and control are now coupled. Although previous studies [13], [14], [15], [16] have investigated the impact of *independent* wave information errors resulting from nonideal WEF estimators or predictors, no study has analyzed such a *coupling* effect between control model error and WEF estimation–prediction error; for instance, the prediction error could be amplified under estimation errors, undermining closed-loop stability. In addition, in previous experimental studies [17], [18], a certain degree of robustness of the MPC system against multiple model mismatch is observed; meanwhile, an artificial adjustment of linear model parameters in control has been used to cope with nonlinearities. Nevertheless, these issues are never systematically examined and clarified.

This study aims to fill this research gap. By examining a complete MPC loop under typical linear and nonlinear model errors, with fundamentally different characteristics, and by further including different WEF estimator/predictor tuning options, it complements the previous study [8] and provides a more comprehensive and complete understanding of WEC control behavior. The main finding is that the sensitivity properties of a WEC MPC controller in isolation can significantly alter, with the addition of an estimation–prediction loop: for system damping-related errors, the control robustness can be slightly *enhanced*, whereas for mass and stiffness errors, performance degradation can be significantly *amplified*. The mechanisms underlying these phenomena are thoroughly analyzed and clarified, and two particularly worrying conditions, an *instability* caused mainly by mass errors and *self-locking* caused by overestimation of body stiffness, are highlighted. Meanwhile, the tradeoffs between accuracy and robustness in WEF estimation and prediction are investigated, which proves crucial to retaining good control performance. Based on these results, this study challenges the "separation principle" underlying most WEC control studies and highlights the importance of examining the complete control system, rather than the isolated controller, in the presence of model errors. This study also offers practical guidelines for WEC control application, including model accuracy requirements, control parameter tuning, and the handling of some nonlinear system dynamics.

The remainder of this article is organized primarily in two parts: the WEC model, MPC controller, and WEF estimator and predictor tuning options are described in Section II, and a comprehensive numerical analysis is presented in Section III.

II. WEC Model and WEC Control System

A. Equation of Motion

This study is based on a heaving point absorber, which is the most representative and widely used in control research. The system equation can be described as

$$M\ddot{z}(t) = f_e(t) + f_g(t) + f_{\text{rad}}(t) + f_{\text{hs}}(t) + f_{\text{lin,fric}}(t) + f_{\text{nl,vis}}(t) + f_{\text{nl,coul}}(t) \quad (1)$$

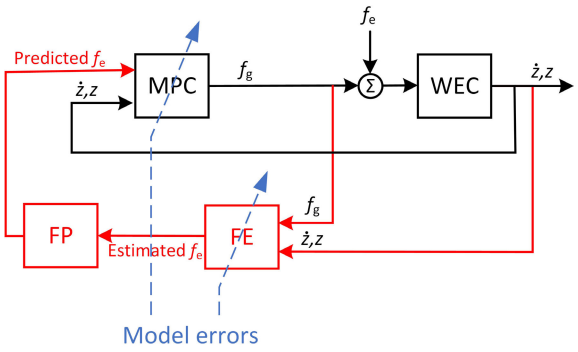

Fig. 1. Schematic of a complete MPC system with WEF estimation (FE) and prediction (FP), and the effect of model error. Note that the calculation of the radiation system state is included in the MPC block.

where t is the continuous time, z, $\dot{z}$, and $\ddot{z}$ are the body displacement, velocity, and acceleration, respectively, M is the body mass, and f_e is the WEF described by

$$f_e(t) = \int_{-\infty}^{\infty} k_e(t-\tau)\eta(\tau)d\tau \quad (2)$$

with η the wave elevation and $k_e(t)$ the wave excitation convolution kernel of the body, f_g is the power take-off (PTO) force, and f_{rad}, f_{hs}, and $f_{\text{lin,fric}}$, respectively, are the radiation, hydro-static, and linear friction forces described by

$$f_{\text{rad}}(t) = -M_\infty \ddot{z}(t) - \int_{-\infty}^{t} k_{\text{r}}(t-\tau)\dot{z}(\tau)d\tau \quad (3)$$

$$f_{\text{hs}}(t) = -Kz(t) \quad (4)$$

$$f_{\text{lin,fric}}(t) = -R_0\dot{z}(t) \quad (5)$$

where M_∞ is the added mass at infinite frequency, $k_{\text{r}}(t)$ is the radiation convolution kernel, K is the hydro-stiffness, and R_0 is a linear friction coefficient. Using a state-space representation of the radiation convolution

$$\dot{\xi}(t) = A_{\text{r,c}}\xi(t) + B_{\text{r,c}}\dot{z}(t)$$
$$\int_{-\infty}^{t} k_{\text{r}}(t-\tau)\dot{z}(\tau)d\tau = C_{\text{r}}\xi(t) \quad (6)$$

where $\xi \in \mathbb{R}^m$ is the m-dimensional radiation subsystem state, and $A_{\text{r,c}}$, $B_{\text{r,c}}$, and C_{r} are the associated matrices, which can be obtained using system identification toolboxes (see [19]).

Regarding the nonlinear forces, $f_{\text{nl,vis}}$ is the viscous drag force [6]

$$f_{\text{nl,vis}}(t) = -0.5\rho\pi a^2 C_d|\dot{z}(t)|\dot{z}(t) \quad (7)$$

where ρ is the water density, a is the body radius, C_d is the drag coefficient, and $f_{\text{nl,coul}}$ is the nonlinear part of mechanical friction, which mainly contains a Coulomb force [6], also termed the static friction force

$$f_{\text{nl,coul}}(t) = -\text{sign}(\dot{z})F_{\text{c}} \quad (8)$$

where F_{c} is the magnitude of static friction force.

In this study, the WEF estimator and MPC controller are always designed based on the linear system, i.e., (1) with $f_{\text{nl,vis}} = 0$ and $f_{\text{nl,coul}} = 0$. With the state-space description of

radiation convolution equation (6), the linear system can be described by

$$\dot{x}(t) = A_c x(t) + B_c f_e(t) + B_c f_g(t)$$
$$y(t) = Cx(t) \tag{9}$$

where $x = [\dot{z}, z, \xi^T]^T \in \mathbb{R}^n$ is the n-dimensional state, $n = m+2$, $y = [\dot{z}, z]^T \in \mathbb{R}^2$ is the system output consisting of the measurable body velocity and position, and

$$A_c = \begin{bmatrix} -\frac{R_0}{M+M_\infty} & -\frac{K}{M+M_\infty} & -\frac{C_r}{M+M_\infty} \\ 1 & 0 & 0_{m\times 1} \\ B_{r,c} & 0_{1\times m} & A_{r,c} \end{bmatrix}, \quad B_c = \begin{bmatrix} \frac{1}{M+M_\infty} \\ 0 \\ 0_{m\times 1} \end{bmatrix}$$
$$C = \begin{bmatrix} 1 & 0 & 0_{1\times m} \\ 0 & 1 & 0_{1\times m} \end{bmatrix}. \tag{10}$$

In this study, the considered WEC is a cylinder buoy with a radius of 2 m and a draft of 2 m; the mass is $M = 25.13 \times 10^3$ kg, the stiffness is $K = 123.15$ kN/m, and the linear damping coefficient is set to $R_0 = 2$ kN/(m/s). The hydrodynamic parameters are calculated using NEMOH [20]. The drag coefficient is assumed to be $C_d = 1$ [21]. The static friction force magnitude is set to be $F_c = 6$ kN. The wave condition is modeled using the Bretschneider spectrum with a significant wave height of 1 m and a peak period of 6 s. Note that, although the numerical case study is carried out for a specific set of wave/WEC parameters, generic sensitivity mechanisms can be revealed from the analysis.

B. WEF Estimation

With the system model known, the instantaneous WEF can be regarded as an unknown state of the system and estimated based on measurable states and the control force. There exist a number of estimator options, among which the Kalman filter (KF) with harmonic oscillator (KFHO) is representative and mostly used, capable of achieving very good accuracy [9], and thus is selected in this study. The KFHO is based on a discretized model

$$x[k+1] = Ax[k] + Bf_e[k] + Bf_g[k]$$
$$y[k] = Cx[k] \tag{11}$$

where k is the discrete time step, with T_s the sampling period, $A = \exp(A_c T_s)$, and $B = A_c^{-1}(A - I)B_c$, obtained from zero-order hold discretization (I denotes the identity matrix). In the KFHO, the WEF is modeled as the sum of multiple sinusoids, which gives the following augmented system:

$$\begin{bmatrix} x[k+1] \\ h[k+1] \end{bmatrix} = \begin{bmatrix} A & BC_h \\ 0_{2L\times n} & A_h \end{bmatrix} \begin{bmatrix} x[k] \\ h[k] \end{bmatrix} + \begin{bmatrix} B \\ 0_{2L\times 1} \end{bmatrix} f_g[k] + \begin{bmatrix} \epsilon_x \\ \epsilon_h \end{bmatrix}$$
$$y[k] = [C \quad 0_{2\times 2L}] \begin{bmatrix} x[k] \\ h[k] \end{bmatrix} + \epsilon_y \tag{12}$$

where $h = [h_1, \dot{h}_1, \ldots, h_L, \dot{h}_L]^T \in \mathbb{R}^{2L}$ is the vector containing L sinusoidal components: h_i are the sinusoidal values, $\dot{h}_i$ are the derivatives, and ω_i are the frequencies, so that

$$A_h = \bigoplus_{i=1}^{L} \exp\left(T_s \begin{bmatrix} 0 & 1 \\ -\omega_i^2 & 0 \end{bmatrix}\right), C_h = 1_{1\times L} \bigotimes [1, 0] \tag{13}$$

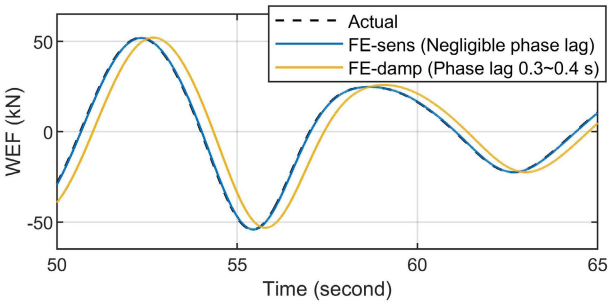

Fig. 2. Illustration of two WEF estimators, with sensitive and damped parameter tuning options (FE-sens and FE-damp), respectively.

where $\bigoplus$ and $\bigotimes$ denote the direct sum of matrices and the Kronecker product. Finally, ϵ_x and ϵ_h are the model noises, ϵ_y is the measurement noise, and the associated covariance matrices are Σ_x, Σ_h, and Σ_y, respectively (the cross-covariance between ϵ_x and ϵ_h is zero). Classical KF algorithms (omitted here) can be applied to obtain the estimate, $\hat{h}$, and the WEF estimate is $\hat{f}_e = C_h \hat{h}$.

The variance of the WEF process, Σ_h, is the key estimator parameter. Generally, a smaller variance represents a higher confidence in the assumed WEF dynamics, that is, a sinusoidal process. In this study, only one frequency component is used, set to be the peak wave frequency. Two WEF estimator tuning options will be examined.

1) *A Sensitive WEF Estimator (FE-Sens):* The KF parameters are $\Sigma_x = \text{diag}[\sigma_{x,1}, \ldots, \sigma_{x,n}]$, $\Sigma_y = \text{diag}[\sigma_{y,1}, \sigma_{y,2}]$, and $\Sigma_h = \text{diag}[\sigma_{h,1}, \sigma_{h,2}]$ (the dimension of h is 2, as only one frequency is used), and are tuned such that, when there is no model error, the estimated WEF tracks the exact value with a negligible time lag, as shown in Fig. 2. This yields a relatively large Σ_h; in other words, the WEF behaves more like a randomized input in the estimation model.
2) *A Damped WEF Estimator (FE-Damp):* In this case, Σ_x and Σ_y remain the same, while the values of Σ_h are reduced such that the estimator, by assuming a sinusoidal model on WEF, exhibits a stronger filtering (or damping) effect and thus is less sensitive. Consequently, the estimated WEF has a dynamical lag of 0.3–0.4 s to the exact WEF, as shown in Fig. 2.

It is recognized that *phase* accuracy has a great impact on energy performance [15], so one can expect that control based on FE-sens performs better than FE-damp. However, it will be shown that when model errors are included, a certain degree of filtering effect is important for closed-loop stability; in other words, there is a tradeoff between accuracy and robustness.

C. WEF Prediction

With the WEF estimate available, future values can be predicted with time-series models based on past values. Linear models, including auto-regressive (AR) models, which apply one-step prediction recursively into the future, and direct multistep (DMS) models, which directly use multistep prediction through matrix multiplication, have been shown to give *equivalent* and optimal prediction accuracy [22]. In this study,

a DMS model obtained from the wave spectrum is considered, due to its theoretical *optimality* for Gaussian waves [23]; almost the same results can be obtained if other options in [22] are used.

Let the WEF spectral density be $S_f(\omega)$, then its auto-covariance function (ACVF), $R_{\rm ff}$, defined as

$$R_{\rm ff}(\tau) = \lim_{T\to\infty} \frac{1}{2T} \int_{-T}^{T} f_e(t) f_e(t+\tau) dt \tag{14}$$

is linked to $S_f(\omega)$ by the Wiener–Khinchin theorem [24]

$$R_{\rm ff}(\tau) = \int_0^{\infty} S_f(\omega) \cos(\omega\tau) d\omega. \tag{15}$$

Note that both $S_f(\omega)$ and $R_{\rm ff}(\tau)$ are the real and even functions. Denote the past (from WEF estimates) and future (forecast) WEF vectors as

$$\begin{aligned} \hat{f}_{e,\rm past} &= \left[\hat{f}_e[k-L_p+1] \cdots \hat{f}_e[k]\right]^{\rm T} \\ \hat{f}_{e,\rm future} &= \left[\hat{f}_e[k+1] \cdots \hat{f}_e[k+L_f]\right]^{\rm T} \end{aligned} \tag{16}$$

with L_p and L_f being the historical and prediction lengths. The optimal prediction is given by

$$\hat{f}_{e,\rm future} = \Sigma_{\rm fp} \Sigma_{\rm pp}^{-1} \hat{f}_{e,\rm past} \tag{17}$$

where $\Sigma_{\rm pp}$ is the auto-covariance matrix of $\hat{f}_{e,\rm past}$, $\Sigma_{\rm fp}$ is the cross-covariance matrix between $\hat{f}_{e,\rm past}$ and $\hat{f}_{e,\rm future}$, and both $\Sigma_{\rm pp}$ and $\Sigma_{\rm fp}$ can be calculated from $R_{\rm ff}$ as follows. Let $r_i = R_{\rm ff}(iT_s)$, assuming $L_f > L_p$, there are

$$\begin{aligned} \Sigma_{\rm pp} &= \begin{bmatrix} r_0 & \cdots & r_{L_p-1} \\ \vdots & \ddots & \vdots \\ r_{L_p-1} & \cdots & r_0 \end{bmatrix} \\ \Sigma_{\rm fp} &= \begin{bmatrix} r_{L_p} & \cdots & r_{L_p+L_p-1} & \cdots & r_{L_p+L_f-1} \\ \vdots & \ddots & \vdots & \cdots & \vdots \\ r_1 & \cdots & r_{L_p} & \cdots & r_{L_f} \end{bmatrix}^{\rm T}. \end{aligned} \tag{18}$$

Note that $\Sigma_{\rm pp} \in \mathbb{R}^{L_p \times L_p}$ and is symmetric, while $\Sigma_{\rm fp} \in \mathbb{R}^{L_f \times L_p}$.

However, in practice, it may turn out that $\Sigma_{\rm pp}$ has a relatively large condition number or is near singular [23]; as a result, the elements of the prediction matrix, $\Sigma_{\rm fp}\Sigma_{\rm pp}^{-1}$, have large magnitude. Consequently, the prediction becomes sensitive to perturbations in its input, i.e., $\hat{f}_{e,\rm past}$, and that is particularly the case in the presence of model errors, which results in WEF estimation errors. Hence, it is *always* necessary to check and control the sensitivity of the prediction matrix. To achieve this, eigendecomposition of [23] is adopted as $\Sigma_{\rm pp} = Q\Lambda Q^{\rm T}$, where $\Lambda = {\rm diag}[\lambda_1, \ldots, \lambda_{L_p}]$ is the diagonal matrix containing the eigenvalues of $\Sigma_{\rm pp}$, and $Q = [q_1, \ldots, q_{L_p}]$ is the matrix containing the corresponding eigenvectors. Eliminating all the eigenvalues with magnitude smaller than a preset threshold, $\lambda_{\rm th}$, yields $\Lambda^* = {\rm diag}[\lambda_1, \ldots, \lambda_{L_{\rm th}}]$ and $Q^* = [q_1, \ldots, q_{L_{\rm th}}]$, where $L_{\rm th}$ is the number of remaining eigenvalues/eigenvectors, and the predictor as

$$\hat{f}_{e,\rm future} = \Sigma_{\rm fp}\left(\Sigma_{\rm pp}^*\right)^{-1} \hat{f}_{e,\rm past} = \Sigma_{\rm fp} Q^* \left(\Lambda^*\right)^{-1} \left(Q^*\right)^{\rm T} \hat{f}_{e,\rm past}. \tag{19}$$

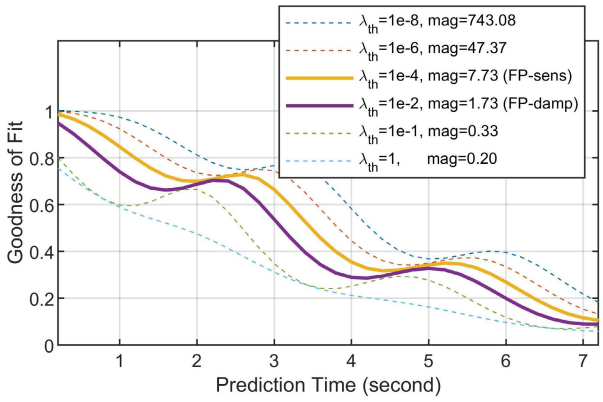

Fig. 3. GoF of WEF predictors with different eigenvalue thresholds $\lambda_{\rm th}$. The coefficient magnitude (mag) is defined as the maximal absolute element values of the prediction matrix, $\Sigma_{\rm fp}(\Sigma_{\rm pp}^*)^{-1}$.

The accuracy of the WEF predictor can be evaluated using the goodness of fit (GoF) index, which is a function of the forecasting step l and defined [10] as

$$\mathcal{G}(l) = 1 - \sqrt{\frac{\sum_k (f_e[k+l] - \hat{f}_e[k+l])^2}{\sum_k (f_e[k+l])^2}}. \tag{20}$$

The choice of $\lambda_{\rm th}$ corresponds to another tradeoff between accuracy and robustness; a small $\lambda_{\rm th}$ gives high accuracy, close to the theoretical optimum in (17), but generates large magnitudes in the prediction matrix elements, as shown in Fig. 3. In such a case, the predictor becomes sensitive to perturbations in $\hat{f}_{e,\rm past}$, i.e., the sequence of the estimated WEF. In this study, two WEF predictor tuning options are examined.

1) *A Sensitive WEF Predictor (FP-Sens):* Based on a relatively small threshold, $\lambda_{\rm th}$ = 1e-4, which gives a coefficient magnitude over 7, as shown in Fig. 3.
2) *A Damped WEF Predictor (FP-Damp):* Based on a larger threshold, $\lambda_{\rm th}$ = 1e-2, which yields a magnitude less than 2, as shown in Fig. 3.

It will be shown later that FE-sens works well with an accurate model, but any model error will lead to consequent errors in WEF estimation and, in such cases, the robustness of the WEF *predictor* turns out to be crucial.

D. Energy-Maximizing MPC

MPC requires full observation of the system state. The radiation system state, ξ, can be easily calculated, e.g., by direct integration of the radiation system

$$\xi[k] = A_{\rm r}\xi[k-1] + B_{\rm r}\dot{z}[k-1] \tag{21}$$

where $A_{\rm r} = \exp(A_{\rm r,c}T_s)$ and $B_{\rm r} = A_{\rm r,c}^{-1}(A_{\rm r} - I)B_{\rm r,c}$. Now, based on the predicted WEF $\hat{f}_e[k], \ldots, \hat{f}_e[k+N-1]$ over a prediction horizon N, and the observed state $x[k]$, the energy-maximizing MPC calculates the optimal control force by solving the following optimization problem:

$$\max_{\bar{f}_g[0],\ldots,\bar{f}_g[N-1]} \sum_{i=0}^{N-1} -\frac{1}{2} T_s \bar{f}_g[i](\bar{x}_1[i] + \bar{x}_1[i+1])$$

$$\begin{aligned}
\text{s.t. } & \bar{x}[i+1] = A\bar{x}[i] + B\bar{f}_e[i] + B\bar{f}_g[i], \\
& i = 0, \ldots, N-1 \\
& -Z_m \le x_2[i] \le Z_m, \quad i = 1, \ldots, N \\
& -F_m \le \bar{f}_g[i] \le F_m, \quad i = 0, \ldots, N-1 \\
& \bar{x}[0] = x[k], \quad \bar{f}_e[i] = \hat{f}_e[k+i], \\
& i = 0, \ldots, N-1
\end{aligned} \tag{22}$$

where $\bar{f}_g[0], \ldots, \bar{f}_g[N-1]$ are the (virtual) control forces to be determined, $\bar{x}[1], \ldots, \bar{x}[N]$ is the corresponding system trajectory, and Z_m and F_m are the displacement and force limits, forming the system operation constraints. Note that the energy is calculated based on zero-order-hold discretization and the trapezoidal rule of integration. Problem (22) is a quadratic program, typically convex, and can thus be solved efficiently with mature algorithms in practice [17]. After solving (22), the first control move is applied to the device, namely, $f_g[k] = \bar{f}_g[0]$ while, at the next step, the optimization is repeated based on the updated information and shifted horizon.

In the case study, simulations are based on MATLAB-Simulink with a sampling time of 0.002 s. Each run of simulation lasts 3 min, so a frequency grid covering the considered wave spectrum, with an interval of 1/180 Hz, is used to generate wave signals, which gives 92 frequency components. Note that although multiple phase realizations, or a relatively long time scale, are usually required for *accurate* power assessment [25], a single-phase realization is used in this study, for computational efficacy, which suffices to give a representative *relative* control comparison; this will be verified in Section III-B. The sampling time for MPC is 0.2 s, and the prediction horizon is $N = 36$, yielding a 7.2-s prediction time, sufficiently long to achieve the optimal performance. Note that the sampling time for MPC is chosen according to the tradeoff between control performance and computation such that, for a given prediction time, a decrease in sampling time (with an increased optimization dimension) does not give a higher energy performance. The MPC optimization is solved using the MATLAB function "quadprog," which is based on an interior-point method [26], and the average computation time is within 0.01 s. For the WEF prediction, there are $L_f = N = 36$ and $L_p = 30$, where L_p is chosen such that the DMS model gives satisfactory prediction accuracy for control. The constraints are set to $Z_m = 2$ m and $F_m = 150$ kN, both active under the optimal condition.

III. Numerical Analysis of Sensitivity

A. Research Method and Preliminary Analysis

In this section, the impact of linear model errors, including errors in the damping R_0, radiation convolution $k_r(t)$, system mass $M + M_\infty$, and stiffness K, will be examined *individually*. For this case, the *actual* system is assumed to only have the linear dynamics, namely, (1) with $f_{\text{nl,vis}}(t) = 0$ and $f_{\text{nl,coul}}(t) = 0$. The system can be described as

$$M_t\ddot{z}(t) + R_0\dot{z}(t) + k_r(t) * \dot{z}(t) + Kz(t) = f_e(t) + f_g(t) \tag{23}$$

where $M_t = M + M_\infty$, and $*$ denotes the convolution. The *control* model, used *both* in WEF estimation and MPC, is assumed to have an error in each parameter, namely, $\Delta R_0 = e_R R_0$, $\Delta k_r(t) = e_{kr} k_r(t)$, $\Delta M_t = e_M M_t$, and $\Delta K = e_K K$, with e_R, e_{kr}, e_M, and e_K being the associated *multiplicative* errors. The considered error ranges are roughly decided based on experience, where the damping-related errors are usually more significant than mass/stiffness errors.

Before numerical investigation, examination of the estimator model form can help illustrate the effect of model errors on WEF estimation. Assume that an "ideal" estimator is used, which has perfect knowledge of $\ddot{z}$, $\dot{z}$, and z, perfect knowledge of all model parameters except R_0, which is now $R_0 + e_R R_0$, and full confidence on the model it uses. The estimator model is

$$\begin{aligned}
& M_t\ddot{z}(t) + (R_0 + e_R R_0)\dot{z}(t) + k_r(t) * \dot{z}(t) + Kz(t) \\
& = f_e(t) + f_g(t)
\end{aligned} \tag{24}$$

giving the following WEF estimate:

$$\begin{aligned}
\hat{f}_e(t) &= M_t\ddot{z}(t) + (R_0 + e_R R_0)\dot{z}(t) + k_r(t) * \dot{z}(t) + Kz(t) \\
&\quad - f_g(t) \\
&= f_e(t) + e_R R_0\dot{z}(t).
\end{aligned} \tag{25}$$

One can see that the damping error appears in the WEF estimate, and the estimation error is exactly the corresponding damping force error, $e_R R_0\dot{z}$. This is not surprising: since the estimator treats the WEF as an arbitrary unknown state, every unmodeled force will be attributed to the WEF. A similar analysis applies to other types of errors.

In this study, the control performance index is the "normalized energy." For a given controller, let the energy generated be E_1, and let the energy generated by the ideal controller (e.g., the controller with ideal WEF estimation, ideal WEF prediction, and no model error) be E_0; the normalized energy is then defined as E_1/E_0. Only in the nonlinear case, the performance is defined as the actual energy generation (represented by the average power), as the "ideal" performance is generally not available (nonlinear MPC cannot be regarded as ideal, due to nonconvexity [27]).

B. Damping Error

Initially, different values of the (multiplicative) damping error, e_R, ranging from -0.75 to 1, are investigated. For each e_R value, simulations are conducted with different WEF estimator and predictor tuning options, and power generation performance is recorded; the result is shown in Fig. 4. Fig. 4(a) shows the impact of e_R on the MPC controller performance *in isolation*, i.e., with ideal WEF estimation and prediction. One can see slight performance degradation (less than 5%) under damping errors. Before proceeding to the analysis, the corresponding results with 16 different phase realizations are presented in Fig. 5. It can be seen that the variation range of performance, originally more than 10% for accurate evaluation of energy generation, compresses to about 1% after being normalized. This verifies that the normalized control performance is much less affected by the phase realization, and

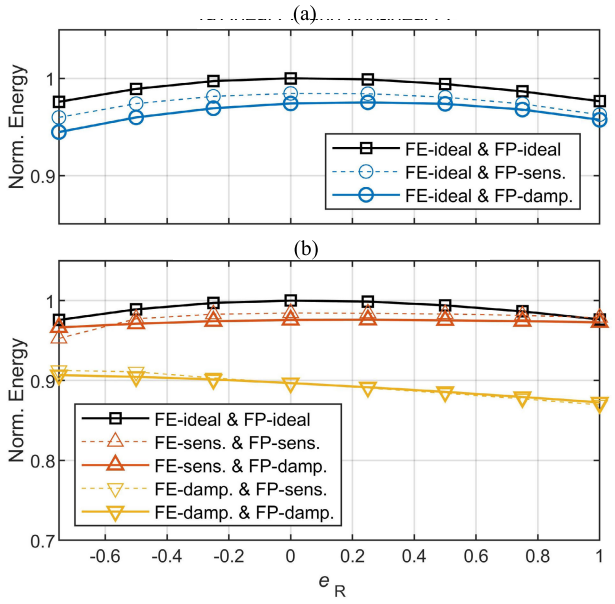

Fig. 4. Impact of damping error on energy generation performance, under different FE/FP tuning options. (a) Ideal FE and nonideal FP. (b) Nonideal FE and nonideal FP.

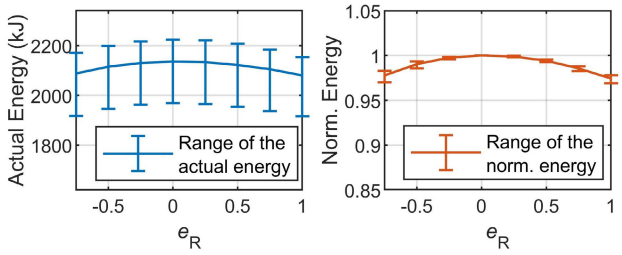

Fig. 5. Mean, minimum, and maximum values of the actual energy generation (left) and normalized energy generation (right) corresponding to the first curve in Fig. 4(a) under 16 different phase realizations.

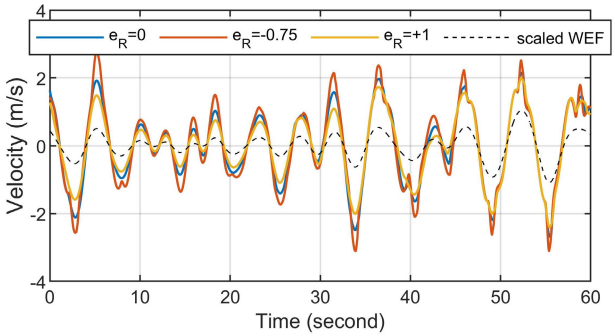

Fig. 6. Velocity profiles with ideal FE and ideal FP, under different damping errors. Note the differences in velocity amplitude.

representative control *comparisons* can be made using a single-phase realization. Looking at the control trajectories in Fig. 6, it can be seen that energy performance degradation comes from the deviations in velocity *amplitude* from the optimum: the velocity curves are "in phase" with the WEF, namely, they have the same zero-crossing and peak time, but, with negative damping errors, the velocity is exaggerated, compared to the optimal velocity profile, and vise versa. This can be explained by the fact that the maximization of energy requires

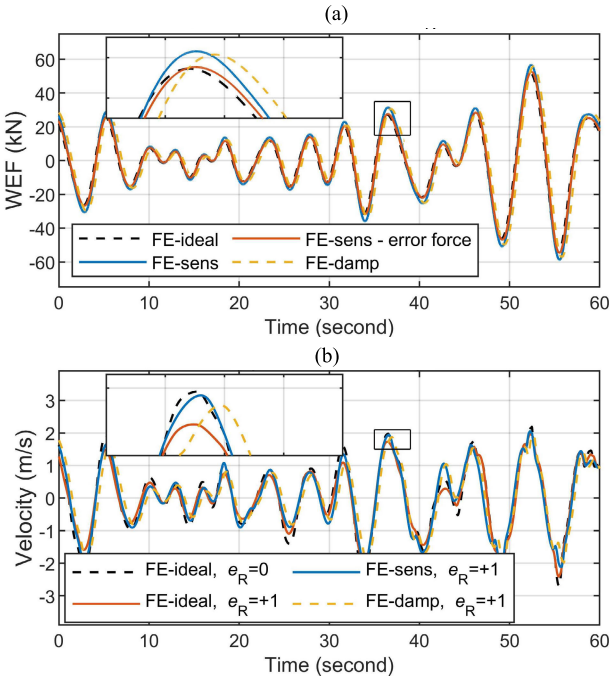

Fig. 7. Estimated WEF and velocity profiles with nonideal FE (and FP-damp), when $e_R = +1$. Note the amplitude-error-canceling effect of FE-sens. (a) Estimated WEF when $e_R = +1$. (b) Controlled velocity.

the body to follow an optimal velocity trajectory. Recall that the unconstrained optimal velocity $V^*(\omega)$, in the frequency domain, is described by

$$V^*(j\omega) = \frac{F_e(j\omega)}{2(R_0 + R_a(\omega))} \tag{26}$$

where $F_e(j\omega)$ and $R_a(\omega)$ are the WEF amplitude and radiation damping at frequency ω, respectively. Under constraints, optimal control trajectories also exhibit behaviors similar to the "amplitude/phase conditions" of the unconstrained optimum [13]. Hence, if there is an overestimation in system damping, the controller is likely to give a lower velocity amplitude. In summary, for the MPC controller alone, the velocity amplitude error resulting from the damping error is the source of performance decrease.

Fig. 4(a) also shows the results when the WEF estimation remains ideal while the effect of nonideal WEF prediction is included. One can see that, in addition to e_R, nonideal WEF prediction, with inevitable WEF prediction errors, yields a further performance decrease, as can be expected. Meanwhile, a sensitive predictor achieves a better energy capture efficiency than a damped one, due to its higher prediction accuracy (see Fig. 3).

In Fig. 4(b), nonideal WEF estimation is further included, thereby forming the complete estimation–prediction loop in Fig. 1. Two important observations can be made: 1) a sensitive WEF estimator yields better energy performance than a damped estimator and 2) under e_R, the performance with a nonideal WEF estimator turns out to be even *better* than that of the ideal case. To investigate these issues, the WEF estimates and the velocity trajectories are plotted in Fig. 7. Fig. 7(a) shows that a damped WEF estimator results in a phase lag in both WEF estimation and the corresponding velocity

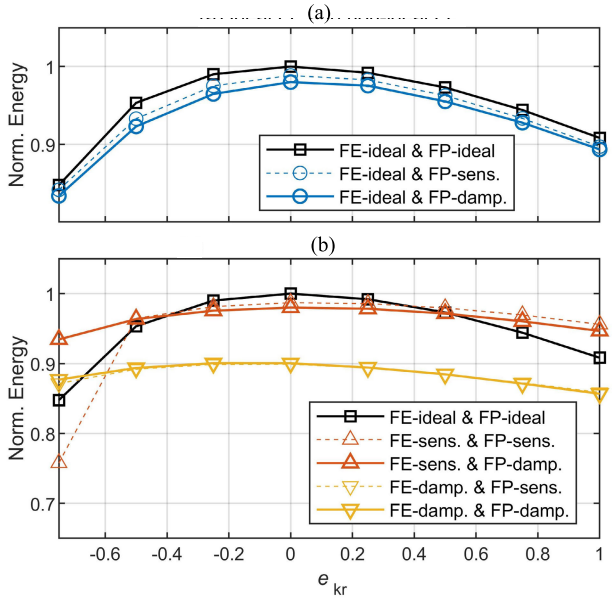

Fig. 8. Impact of radiation convolution error on energy generation performance, under different FE/FP tuning options. (a) Ideal FE and nonideal FP. (b) Nonideal FE and nonideal FP.

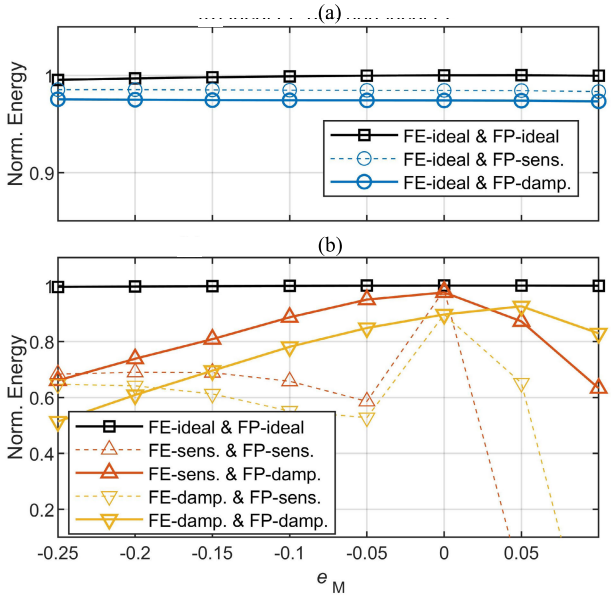

Fig. 9. Impact of mass error on energy generation performance, under different FE/FP tuning options. (a) Ideal FE and nonideal FP. (b) Nonideal FE and nonideal FP.

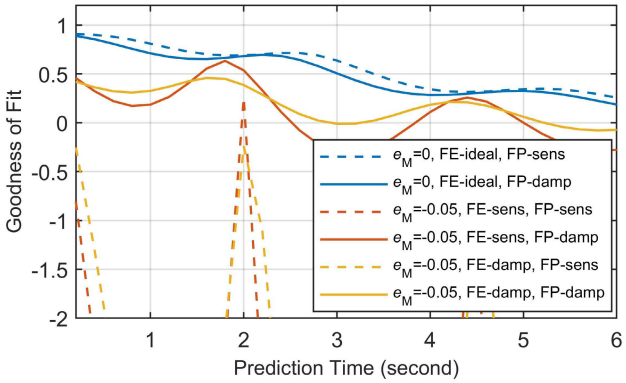

Fig. 10. GoF of WEF prediction under mass errors.

trajectory, as expected in Fig. 2. It has been recognized, e.g., in [15], that energy capture is much more sensitive to phase errors than amplitude errors, so a damped WEF estimator leads to suboptimality. On the other hand, note that with a positive damping error ($e_R = 1$), the estimated WEF [blue line in Fig. 7(a)] has a larger amplitude than the exact value (black dashed line), but without a phase difference. This is because the error force now appears in the WEF estimate, as shown in (24), and since the velocity $\dot{z}$ is controlled to be in phase with the WEF, the damping error force $e_R R_0 \dot{z}$ will only lead to amplitude error in the WEF estimate, without affecting its phase. If this error force is added back (to get the red line), one can see that the original WEF is recovered, so (24) is verified. Hence, now the MPC controller has not only the damping error (overestimation) in its model, which results in a lower velocity amplitude [red line in Fig. 7(b)], but also the WEF error (overestimation) in its input, and the latter effect *cancels* the velocity error to a certain extent [to get the blue line in Fig. 7(b)], namely, the velocity amplitude is less erroneous. A similar analysis applies to the case of a negative damping error.

C. Radiation Force Convolution Error

Next, the impact of e_{kr} ranging from -0.75 to 1 is shown in Fig. 8. Comparing Fig. 8 with Fig. 4, one can see that the impact characteristics of e_{kr} and e_R on energy performance are very similar although the impact of e_{kr} is greater. This can also be explained by (26) since it is the time-domain radiation convolution kernel $k_{\text{r}}(t)$ that contains the effects of frequency-domain radiation damping $R_a(\omega)$, as described by the Ogilvie's relation

$$k_{\text{r}}(t) = \mathcal{F}^{-1}\{R_a(\omega) + j\omega(M_a(\omega) - M_\infty)\} \tag{27}$$

where $\mathcal{F}^{-1}$ denotes the inverse Fourier transform. Hence, e_{kr} also results in errors in the optimal velocity, its impact is greater because the magnitude of $R_a(\omega)$ is larger than R_0 in this case, and, as analyzed in the case of e_R, the joint impact of control and WEF estimation on energy capture under e_{kr} also offset to a certain extent; the mechanisms are generally the same. In addition, it can be seen that when the magnitude of e_{kr} reaches a certain level, e.g., $e_{\text{kr}} = -0.75$, the performance when using a sensitive WEF predictor can degrade seriously compared to a damped predictor. This phenomenon will be further reflected and analyzed in the subsequent investigation of the mass error.

D. Mass Error

The impact of mass error, described by e_M and ranging from -0.25 to 0.1, is shown in Fig. 9. It can be seen, from Fig. 9(a), that the energy performance is rather insensitive to mass error, and this can be explained, again, by (26), as the optimal velocity is independent of the system mass. The result of nonideal wave forecast in Fig. 9(a) is similar to the e_R and e_{kr} cases, and the most concerning result is in Fig. 9(b): when nonideal WEF estimation is included, the performance becomes very sensitive

to the mass error. Particularly, it can be observed that, for both WEF estimator options, when a sensitive WEF predictor is employed, the energy capture typically decreases sharply, even becoming negative (energy consumption). To investigate this phenomenon, the GoF of WEF prediction under different estimator/predictor combinations is plotted in Fig. 10. When the mass is correct, a sensitive WEF predictor is more accurate than a damped one, as in Fig. 3. However, with a mass error involved, the GoF of a damped predictor is less than 0.5 while, for a sensitive predictor, the GoF becomes negative (according to (20), a negative GoF means that the forecasting variance exceeds the variance of the WEF itself).

Accordingly, the control signals are shown in Fig. 11. One can see, from Fig. 11(a), that the mass error results in errors in WEF estimation which, when input to a sensitive WEF predictor, can lead to significant oscillations in the WEF forecast, as shown in Fig. 11(b). Consequently, the control trajectory also oscillates and can be viewed as "unstable," as shown in Fig. 11(c). This *instability* resulting from *perturbation amplification* is the primary cause of the performance degradation apparent in Fig. 9. To tackle this, some damping effects should be introduced, particularly to the WEF forecasting process. As shown in Fig. 11(b), a damped WEF predictor can significantly reduce the oscillations in WEF prediction so that some performance can be recovered in Fig. 9(b). In addition, a damped WEF estimator can also help offset WEF estimation errors, as shown in Fig. 11(a), so that it can sometimes outperform, in terms of energy capture, a sensitive WEF estimator in Fig. 9(b), but this effect is limited.

When a damped DMS model is employed so that instability is avoided in the WEF forecast, the decrease in control performance (red and yellow solid lines in Fig. 9) is mainly due to the phase error of WEF estimation. This will be discussed next, together with the stiffness error case.

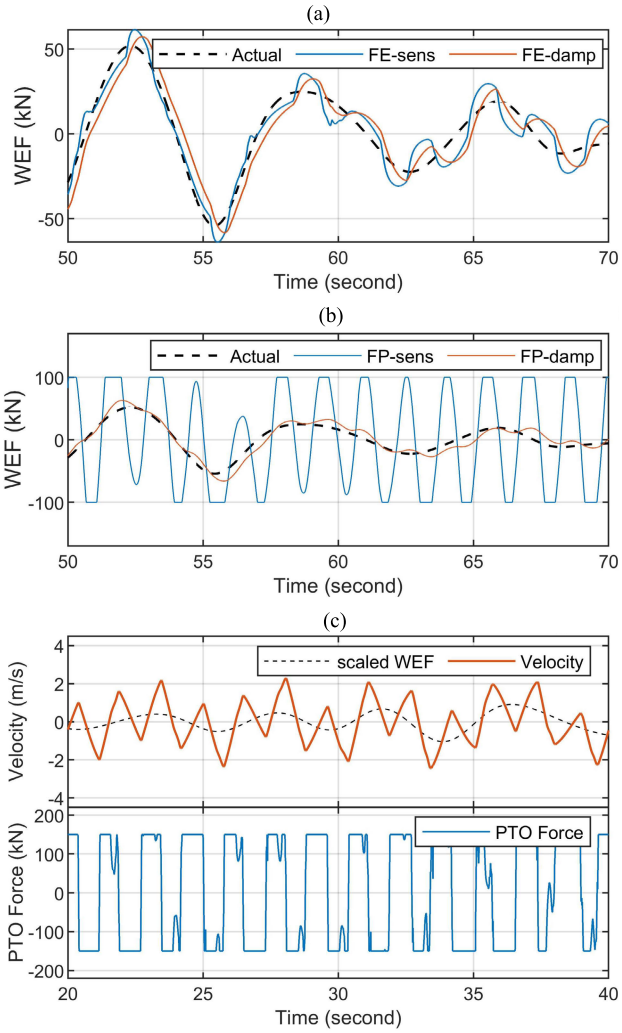

Fig. 11. Example of estimated WEF, predicted WEF, and control trajectory under a mass error. Note the instability phenomenon under a sensitive WEF predictor. (a) Estimated WEF when $e_M = -0.05$. (b) Predicted WEF (1.6 s ahead) under FE-sens when $e_M = -0.05$. (c) Control trajectory under FE-sens and FP-sens when $e_M = -0.05$.

E. Stiffness Error

The impact of a stiffness error, e_K ranging from -0.2 to 0.2, is shown in Fig. 12. From Fig. 12(a), one can see a slight energy performance decrease due to model error. As for the case of mass (both mass and stiffness are imaginary terms in the system intrinsic impedance), the stiffness does not appear in the optimal velocity expression in (26) either, so this performance degradation is likely to be caused by the control force limitation F_m, which restricts the control ability to track the optimal velocity profile. To verify this, the result under unconstrained force is further shown in Fig. 12(a), and an insensitivity to error can now be observed.

However, with a nonideal WEF estimation–prediction loop involved, significant performance decreases are observed again, as shown in Fig. 12(b). The control trajectories under a *negative* stiffness error are shown in Fig. 13(a). In contrast to Fig. 11, there is no significant oscillation, so instability is not the primary cause of the poor energy performance as in the mass error case. Instead, it can be seen that the estimated WEF exhibits a clear phase (leading) error, as does the corresponding WEC velocity. This is because, as analyzed earlier, the stiffness error will be reflected in the WEF estimate. Since the buoyancy force is proportional to the body displacement, thus 90° out of phase with the velocity, and is generally large in amplitude, it has a significant impact on the WEF phase; this explains the performance degradation on the left side of Fig. 12(b). A similar analysis is applicable to the case of mass error with a damped WEF predictor in Fig. 9. In addition, oscillations in prediction occur again when e_K is relatively large (e.g., $e_K = -0.2$), for which the use of a sensitive WEF predictor should be avoided.

On the other hand, the results under a *positive* stiffness error are shown in Fig. 13(b), and a rather interesting phenomenon can be observed: the controller keeps applying the maximum negative force, and the body position remains consistently negative. The explanation is as follows: due to the overestimation of the buoyancy force, which is directed upward, the WEF estimator believes, in order to explain the body motion, that there exists an external force going downward, and this force is attributed to the WEF. Consequently, the estimated WEF has a negative bias, and if the stiffness error is relatively large (e.g., $e_K = 0.1$), the *total* WEF estimate will be negative.

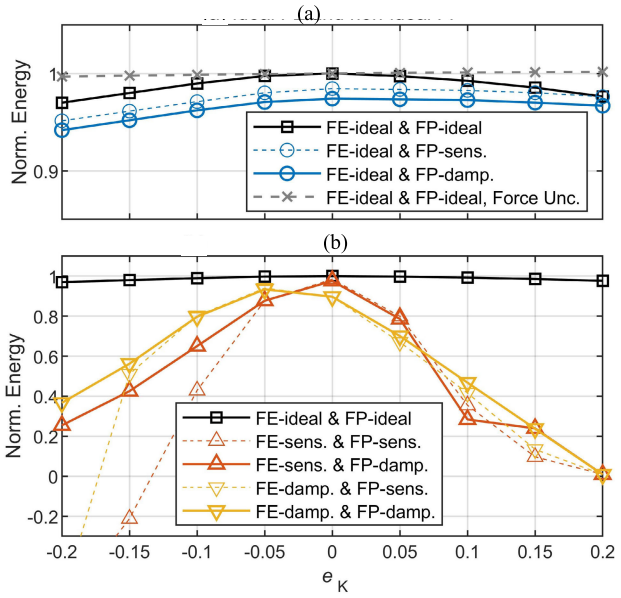

Fig. 12. Impact of stiffness error on energy generation performance, under different FE/FP tuning options. Unc.: Unconstrained. (a) Ideal FE and nonideal FP. (b) Nonideal FE and nonideal FP.

On the other hand, the MPC controller needs to drive the body to move in phase with the WEF, so the WEC now needs to *further go down* and, in order to do so, the force is kept at its negative limit. This is an *irrecoverable* situation, with the PTO force at its constraint or, in an unconstrained situation, the body will be locked at its negative maximum position. This is termed the *self-locking* behavior which, together with the phase error, explains the performance degradation of the right side of Fig. 12(b).

F. Unmodeled Nonlinear Forces

Finally, the impact of two nonlinear forces, namely, a quadratic viscous force $f_{\text{nl,vis}}$ and a static friction force $f_{\text{nl,coul}}$ are examined individually. For the $f_{\text{nl,vis}}$ case, the actual system is assumed to have the linear dynamics plus $f_{\text{nl,vis}}$ only, namely, (1) with $f_{\text{nl,coul}} = 0$; similarly, for the $f_{\text{nl,coul}}$ case, the actual system is (1) with $f_{\text{nl,vis}} = 0$. On the other hand, the estimator and MPC are always based on a linear model; in this way, the MPC maintains a quadratic programming optimization. Note that a nonlinear MPC controller based on a nonlinear system model is computationally challenging and suffers from nonconvexity [1] (that is particularly the case when the *discontinuous* $f_{\text{nl,coul}}$ is involved). Hence, a practical technique is to approximate the nonlinear effects through scheduling of linear *representative* models [28]. The use of linear MPC in nonlinear systems has been shown to be very effective, achieving performance comparable to, or even better than, nonlinear MPC [27]. In this study, since $f_{\text{nl,vis}}$ and $f_{\text{nl,coul}}$ are both velocity-dependent, the tuning of the linear damping coefficient, R_0, will be investigated: the parameter R_0 used in the control model is adjusted by $\Delta R_0 = \alpha_R R_0$, with α_R the tuning coefficient. The results are presented in Fig. 14.

From Fig. 14(a), one can see that, under the effect of the viscous force, MPC performs rather poorly when no adjustment of R_0 is applied. By increasing R_0, the energy

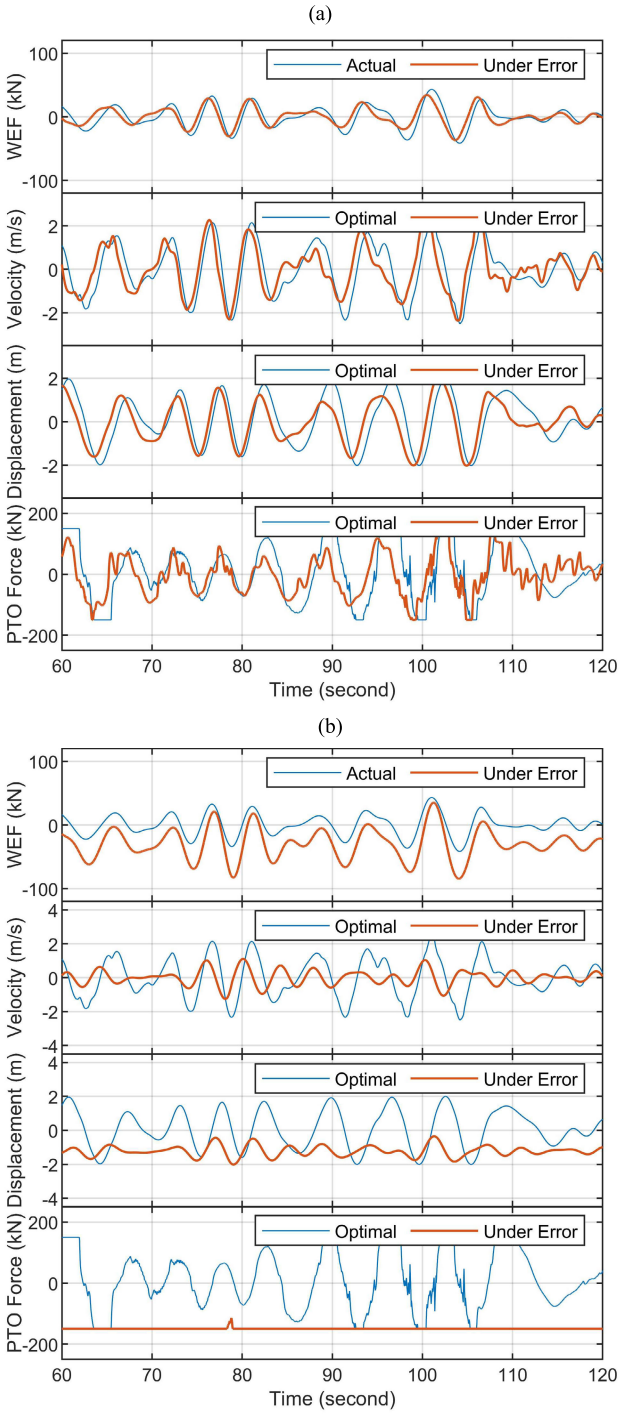

Fig. 13. Control trajectories under positive and negative stiffness errors. Note the velocity phase error in the former case and the self-locking behavior in the latter case. Also note that some abrupt oscillations in the PTO force profile are partly due to the constrained MPC behavior and partly due to the near-positive-semidefiniteness of the quadratic program; these oscillations do not affect the final energy performance. (a) Control trajectory using FE-sens and FP-damp, when $e_K = -0.1$. (b) Control trajectory using FE-sens and FP-damp, when $e_K = +0.1$.

performance is significantly improved, and there exists an optimal value of R_0, at which the nonlinear viscous force is best represented by a linear damper. Moreover, similar to the damping error case, the performance degradation effect is mitigated with a complete WEF estimation–prediction loop, and the explanation is also similar: neglecting the

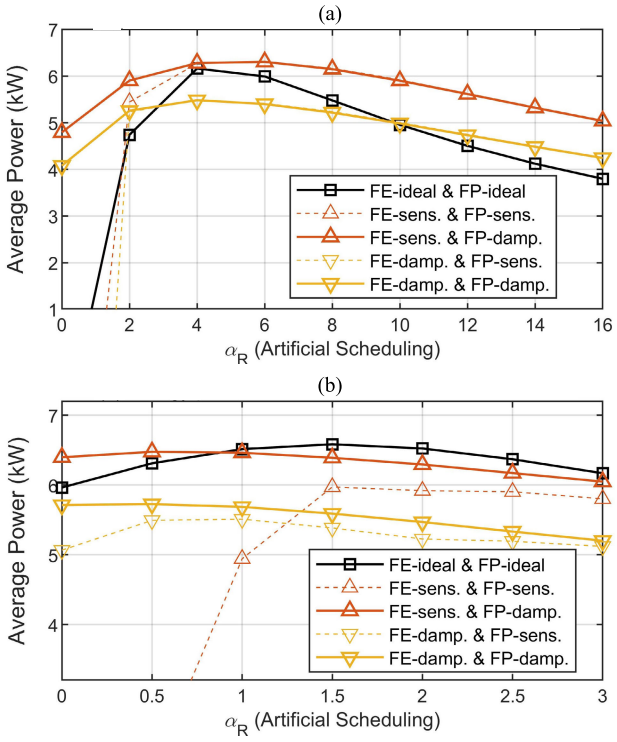

Fig. 14. Impacts of the nonlinear viscous and static friction forces on energy generation performance, under different FE/FP tuning options and different, artificially scheduled linear damping coefficients α_R. (a) Energy performance under nonlinear viscous force. (b) Energy performance under nonlinear static friction.

viscous force can be viewed as an underestimation of system damping.

From Fig. 14(b), the impact of static friction is similar to and relatively smaller than the viscous force, and proper scheduling of R_0 also helps to improve the power capture. In addition, it can be seen both in Fig. 14(a) and (b) that, when the unmodeled nonlinear force is large enough, instability occurs again for a sensitive WEF predictor. In general, these results partly explain the observed robustness of a linear MPC system in wave tank testing [17], [18], where the buoy is experiencing rather large nonlinear effects: the effectiveness of damping adjustment in control-oriented modeling, as well as the error canceling effect of the estimation loop, both contribute to the successful implementation [17], [18].

IV. Conclusion

In this study, the model error sensitivity of the complete WEC MPC system, with WEF estimation and prediction, is analyzed numerically. It is highlighted that, for such a system, it is not only the MPC solution that is affected by model errors, but also the WEF estimate, in which any unmodeled force will be reflected, and this estimation error will propagate through the WEF predictor and ultimately arrive at the MPC input. Consequently, under the *joint* impact of these factors, the complete MPC system shows considerably different behavior than an *isolated* MPC controller.

For an MPC controller in isolation, the energy performance is mainly affected by errors in system damping, including linear damping, the radiation convolution kernel, and the nonlinear viscous and static friction effects, and the degree of impact depends on the magnitude of these error forces. On the other hand, the energy capture generally remains insensitive to errors in mass and stiffness (consistent with [8]). It is shown that energy-maximizing MPC behaves somewhat like an optimal velocity-tracking controller, for which overestimation of damping results in underestimation of the optimal velocity amplitude, and vice versa; in addition, constraints in PTO force may affect the performance by restricting velocity tracking capability. Regarding WEF information requirements, higher WEF prediction accuracy achieves higher power capture efficiency, as can be expected.

However, when nonideal WEF estimation is involved, thereby closing the estimation-prediction control loop, energy performance degradation is generally *mitigated* under damping-related errors and significantly *amplified* under mass or stiffness errors.

1) For damping-related errors, including errors in the linear damping, radiation convolution, viscous force, and static friction, errors in the WEF estimate can *cancel* the errors in optimal velocity profile to a certain extent, so that the energy performance improves compared to an MPC controller in isolation.
2) Errors in mass and stiffness, although not affecting the system damping, can lead to phase errors in the WEF estimate and, consequently, the controlled body velocity, so that the power capture efficiency is significantly degraded.
3) In addition to 1) and 2), for mass or other errors that result in relatively large errors in the WEF estimate, an accurate/sensitive WEF predictor, with a large coefficient magnitude, can produce significant oscillations in the WEF forecast, making the overall control system *unstable*. In this situation, some damping (or filtering) effects introduced, mainly by the use of a damped WEF predictor with a smaller coefficient magnitude, can greatly mitigate the instability effects. Note that such damping effects in WEF prediction (lower forecasting accuracy) are generally considered to be suboptimal when there is no model error, but now prove vital to the system performance.
4) In addition to 1) and 2), under a positive stiffness error, the system can be dominated by a *self-locking* effect, where the controller pushes the body in one direction for all time.

Hence, the results show that the "separation principle" of WEF estimation/prediction and WEC control no longer holds in the presence of model errors. A quite robust, isolated WEC controller can become overly sensitive with an estimation–prediction loop involved; specifically, the detrimental instability and self-locking effects cannot be observed from an MPC controller in isolation.

Finally, some practical guidelines can be drawn for WEC control designers.

1) It is vital to have an accurate mass and stiffness identification, in order to avoid significant energy performance degradation or even device damage.

2) Since some model errors are inevitable, it is important to restrict the coefficient magnitude of the WEF *predictor*, e.g., to be less than 2, to avoid undesirable oscillations. Accuracy needs to be balanced with sensitivity issues.
3) Similarly, the sensitiveness of the WEF *estimator* is another degree of freedom to be tuned, also related to the accuracy–robustness tradeoff.
4) To handle nonlinear viscous and static friction effects within a linear MPC framework, an effective approach to improving the performance is through proper tuning of the linear damping coefficient.

The goal of this article is to reveal some common problems existing in WEC control systems, through a limited, yet representative, case study. The examination is based on a widely used linear model, i.e., Cummins' equation [4], with a multiplicative model error assumption, and with some nonlinear extensions. Other types of modeling errors, such as errors in black-box models (or other models with parameterizations different from Cummins' equation) obtained from system testing data, as well as other nonlinear effects (e.g., nonlinear Froude–Krylov forces), may have different impacts on control. Meanwhile, the results are based on a typical, KFHO-based WEF estimator, with only one frequency component. Other estimation algorithm options and estimator parameter setting options may exhibit different dynamic characteristics, affecting the control performance. In addition, uncertainties in the incident wave spectrum may have a further impact on the WEF forecast. These aspects are worthy of further study in the future.

REFERENCES

[1] J. V. Ringwood, S. Zhan, and N. Faedo, "Empowering wave energy with control technology: Possibilities and pitfalls," *Annu. Rev. Control*, vol. 55, pp. 18–44, Jan. 2023.

[2] J. Hals, J. Falnes, and T. Moan, "A comparison of selected strategies for adaptive control of wave energy converters," *J. Offshore Mech. Arctic Eng.*, vol. 133, no. 3, Aug. 2011, Art. no. 031101.

[3] N. Faedo, S. Olaya, and J. V. Ringwood, "Optimal control, MPC and MPC-like algorithms for wave energy systems: An overview," *IFAC J. Syst. Control*, vol. 1, pp. 37–56, Sep. 2017.

[4] W. Cummins, "The impulse response function and ship motions," *Schiffstechnik*, vol. 9, pp. 101–109, Oct. 1962.

[5] A. Mérigaud, J.-C. Gilloteaux, and J. V. Ringwood, "A nonlinear extension for linear boundary element methods in wave energy device modelling," in *Proc. 31st Int. Conf. Offshore Mech. Arctic Eng.*, vol. 44915, Rio de Janeiro, Brazil, 2012, pp. 615–621.

[6] B. Guo, R. Patton, S. Jin, J. Gilbert, and D. Parsons, "Nonlinear modeling and verification of a heaving point absorber for wave energy conversion," *IEEE Trans. Sustain. Energy*, vol. 9, no. 1, pp. 453–461, Jan. 2018.

[7] Z. Liao et al., "Modelling and control tank testing validation for attenuator type wave energy converter—Part I: Experiment setup and control-oriented modelling," *IEEE Trans. Sustain. Energy*, vol. 14, no. 3, pp. 1747–1757, Jul. 2023.

[8] J. V. Ringwood, A. Mérigaud, N. Faedo, and F. Fusco, "An analytical and numerical sensitivity and robustness analysis of wave energy control systems," *IEEE Trans. Control Syst. Technol.*, vol. 28, no. 4, pp. 1337–1348, Jul. 2020.

[9] Y. Peña-Sanchez, C. Windt, J. Davidson, and J. V. Ringwood, "A critical comparison of excitation force estimators for wave-energy devices," *IEEE Trans. Control Syst. Technol.*, vol. 28, no. 6, pp. 2263–2275, Nov. 2020.

[10] F. Fusco and J. V. Ringwood, "Short-term wave forecasting for real-time control of wave energy converters," *IEEE Trans. Sustain. Energy*, vol. 1, no. 2, pp. 99–106, Jul. 2010.

[11] J.-C. Gilloteaux and J. Ringwood, "Influences of wave directionality on a generic point absorber," in *Proc. 8th Eur. Wave Tidal Energy Conf.*, vol. 8, Uppsala, Sweden, 2009, pp. 1–10.

[12] T. T. Georgiou and A. Lindquist, "The separation principle in stochastic control, redux," *IEEE Trans. Autom. Control*, vol. 58, no. 10, pp. 2481–2494, Oct. 2013.

[13] J. Hals, J. Falnes, and T. Moan, "Constrained optimal control of a heaving buoy wave-energy converter," *J. Offshore Mech. Arctic Eng.*, vol. 133, no. 1, Feb. 2011, Art. no. 011401.

[14] F. Fusco and J. V. Ringwood, "A study of the prediction requirements in real-time control of wave energy converters," *IEEE Trans. Sustain. Energy*, vol. 3, no. 1, pp. 176–184, Jan. 2012.

[15] L. Li, Z. Yuan, Y. Gao, and X. Zhang, "Wave force prediction effect on the energy absorption of a wave energy converter with real-time control," *IEEE Trans. Sustain. Energy*, vol. 10, no. 2, pp. 615–624, Apr. 2019.

[16] N. Faedo, G. Mattiazzo, and J. V. Ringwood, "Robust energy-maximising control of wave energy systems under input uncertainty," in *Proc. Eur. Control Conf. (ECC)*, London, U.K., Jul. 2022, pp. 614–619.

[17] Z. Lin, X. Huang, and X. Xiao, "Fast model predictive control system for wave energy converters with wave tank tests," *IEEE Trans. Ind. Electron.*, vol. 70, no. 7, pp. 6887–6897, Jul. 2023.

[18] Z. Lin, X. Huang, and X. Xiao, "Experimental validation of rollout-based model predictive control for wave energy converters on a two-body, taut-moored point absorber prototype," in *Proc. Eur. Wave Tidal Energy Conf.*, vol. 15, Bilbao, Spain, 2023, p. 174.

[19] D. R. Herber and J. T. Allison, "Approximating arbitrary impulse response functions with Prony basis functions," Eng. Syst. Des. Lab., Urbana, IL, USA, Tech. Rep. UIUC-ESDL-2019-01, 2019.

[20] A. Babarit and G. Delhommeau, "Theoretical and numerical aspects of the open source BEM solver NEMOH," in *Proc. 11th Eur. Wave Tidal Energy Conf.*, Nantes, France, 2015, pp. 1–14.

[21] F. Fusco and J. V. Ringwood, "Hierarchical robust control of oscillating wave energy converters with uncertain dynamics," *IEEE Trans. Sustain. Energy*, vol. 5, no. 3, pp. 958–966, Jul. 2014.

[22] Y. Peña-Sanchez, A. Mérigaud, and J. V. Ringwood, "Short-term forecasting of sea surface elevation for wave energy applications: The autoregressive model revisited," *IEEE J. Ocean. Eng.*, vol. 45, no. 2, pp. 462–471, Apr. 2020.

[23] A. Mérigaud and J. V. Ringwood, "Incorporating ocean wave spectrum information in short-term free-surface elevation forecasting," *IEEE J. Ocean. Eng.*, vol. 44, no. 2, pp. 401–414, Apr. 2019.

[24] M. K. Ochi, *Ocean Waves: The Stochastic Approach*. Cambridge, U.K.: Cambridge Univ. Press, 2005.

[25] A. Mérigaud, "A harmonic balance framework for the numerical simulation of non-linear wave energy converter models in random seas," Ph.D. dissertation, Dept. Electron. Eng., Maynooth Univ., Maynooth, Ireland, 2018.

[26] A. Altman and J. Gondzio, "Regularized symmetric indefinite systems in interior point methods for linear and quadratic optimization," *Optim. Methods Softw.*, vol. 11, nos. 1–4, pp. 275–302, Jan. 1999.

[27] M. Richter, M. E. Magana, O. Sawodny, and T. K. A. Brekken, "Nonlinear model predictive control of a point absorber wave energy converter," *IEEE Trans. Sustain. Energy*, vol. 4, no. 1, pp. 118–126, Jan. 2013.

[28] J. Davidson, S. Giorgi, and J. V. Ringwood, "Linear parametric hydrodynamic models for ocean wave energy converters identified from numerical wave tank experiments," *Ocean Eng.*, vol. 103, pp. 31–39, Jul. 2015.

Zechuan Lin (Student Member, IEEE) was born in Fujian, China, in 1996. He received the B.E. degree in electrical engineering from North China Electrical Power University, Beijing, China, in 2019. He is currently pursuing the Ph.D. degree in electrical engineering with Tsinghua University, Beijing.

From September 2023 to January 2024, he was with the Centre for Ocean Energy Research, Maynooth University, Maynooth, Ireland, where he was a Visiting Student. His research focuses on control and control co-design of wave energy converters.

Xuanrui Huang (Member, IEEE) was born in Xinjiang, China, in 1991. He received the B.E. and Ph.D. degrees in electrical engineering from Tsinghua University, Beijing, China, in 2013 and 2020, respectively.

He is currently a Postdoctoral Researcher with the Department of Electrical Engineering, Tsinghua University. His research focuses on permanent magnet synchronous motor control, wave energy, and switched reluctance machines.

Xi Xiao (Member, IEEE) was born in Hunan, China, in 1973. He received the B.E., M.E., and Ph.D. degrees in electrical engineering from Saint Petersburg State Technical University, Saint Petersburg, Russia, in 1995, 1997, and 2000, respectively.

Since 2001, he has been with the Department of Electrical Engineering, Tsinghua University, Beijing, China, where he is currently a Full Professor. His main areas of research interest are permanent magnet synchronous motor control, power electronics, and renewable energy.

John V. Ringwood (Fellow, IEEE) received the Diploma degree in electrical engineering from Technological University, Dublin, Ireland, in 1981, and the Ph.D. degree in control systems from Strathclyde University, Glasgow, U.K., in 1985.

He was with the School of Electronic Engineering, Dublin City University, Dublin, from 1985 to 2000. He has held visiting positions at Massey University, Auckland, New Zealand, and The University of Auckland, Auckland. He was the Founding Head of the Department of Electronic Engineering, Maynooth University, Ireland, where he served as the Dean of engineering, from 2001 to 2006, and is currently a Chair Professor of electronic engineering and the Director of the Centre for Ocean Energy Research. He has co-authored the monograph *Hydrodynamic Control of Wave Energy Devices* (with Umesh Korde). His research interests focus on control systems and their applications, including renewable energy systems (and wave energy in particular), physiology, and exercise physiology.

Dr. Ringwood was a co-recipient of the IEEE 2016 Control Systems Outstanding Paper Award and the 2023 IEEE Transactions on Control Systems Technology Outstanding Paper Award. He is an Associate Editor of IEEE TRANSACTIONS ON SUSTAINABLE ENERGY, the *Journal of Ocean Engineering and Marine Energy*, and *IET Renewable Power Generation*. He is a Chartered Engineer and a fellow of Engineers Ireland.